

2-7-2024

Experimental study on shear strength of unsaturated soil over a wide suction range and its prediction

Geng NIU

School of Science, Qingdao University of Technology, Qingdao, Shandong 266520, China; State Key Laboratory of Geomechanics and Geotechnical Engineering, Institute of Rock and Soil Mechanics, Chinese Academy of Sciences, Wuhan, Hubei 430071, China, niugeng@qut.edu.cn

Xiao-feng ZHU

School of Science, Qingdao University of Technology, Qingdao, Shandong 266520, China

Jun-xing LI

School of Science, Qingdao University of Technology, Qingdao, Shandong 266520, China

Meng-yuan LÜ

School of Science, Qingdao University of Technology, Qingdao, Shandong 266520, China

See next page for additional authors

Follow this and additional works at: <https://rocksoilmech.researchcommons.org/journal>



Part of the [Geotechnical Engineering Commons](#)

Recommended Citation

NIU, Geng; ZHU, Xiao-feng; LI, Jun-xing; LÜ, Meng-yuan; AN, Li-qi; and CHEN, Zi-han (2024) "Experimental study on shear strength of unsaturated soil over a wide suction range and its prediction," *Rock and Soil Mechanics*: Vol. 44: Iss. 12, Article 1.

DOI: 10.16285/j.rsm.2022.7005

Available at: <https://rocksoilmech.researchcommons.org/journal/vol44/iss12/1>

This Article is brought to you for free and open access by Rock and Soil Mechanics. It has been accepted for inclusion in Rock and Soil Mechanics by an authorized editor of Rock and Soil Mechanics.

Experimental study on shear strength of unsaturated soil over a wide suction range and its prediction

Abstract

In this paper, the experimental studies on the water retention and strength properties of unsaturated weakly expansive soil in a wide suction range were carried out, and a strength model of unsaturated soil over a wide suction range was proposed. The results show that in the wide suction range, the stress–strain curve increases with the increase of suction. The strain hardening occurs in the low suction range, while the strain softening appears in the high suction range. In the low suction range, the sample presents shear contraction, while in the high suction range, the sample begins to show a shear dilation trend at the axial strain of 2%. In addition, a soil-water retention curve model was proposed to distinguish adsorbed water from capillary water, assuming that the strength increment caused by suction is mainly determined by capillary water. The degree of saturation of capillary water was used to replace the effective stress coefficient and then it was substituted into the Bishop's unsaturated soil strength formula. The proposed model was verified by test data of various soil types and compared with the models in the literature. The results show that the proposed model can well describe the strength of unsaturated soil in a wide suction range.

Keywords

unsaturated soil, shear strength, soil-water retention curve, effective stress coefficient, wide suction range

Authors

Geng NIU, Xiao-feng ZHU, Jun-xing LI, Meng-yuan LÜ, Li-qi AN, and Zi-han CHEN

Experimental study on shear strength of unsaturated soil over a wide suction range and its prediction

NIU Geng^{1,2}, ZHU Xiao-feng¹, LI Jun-xing¹, LÜ Meng-yuan¹, AN Li-qi¹, CHEN Zi-han¹

1. School of Science, Qingdao University of Technology, Qingdao, Shandong 266520, China

2. State Key Laboratory of Geomechanics and Geotechnical Engineering, Institute of Rock and Soil Mechanics, Chinese Academy of Sciences, Wuhan, Hubei 430071, China

Abstract: In this paper, the experimental studies on the water retention and strength properties of unsaturated weakly expansive soil in a wide suction range were carried out, and a strength model of unsaturated soil over a wide suction range was proposed. The results show that in the wide suction range, the stress–strain curve increases with the increase of suction. The strain hardening occurs in the low suction range, while the strain softening appears in the high suction range. In the low suction range, the sample presents shear contraction, while in the high suction range, the sample begins to show a shear dilation trend at the axial strain of 2%. In addition, a soil-water retention curve model was proposed to distinguish adsorbed water from capillary water, assuming that the strength increment caused by suction is mainly determined by capillary water. The degree of saturation of capillary water was used to replace the effective stress coefficient and then it was substituted into the Bishop’s unsaturated soil strength formula. The proposed model was verified by test data of various soil types and compared with the models in the literature. The results show that the proposed model can well describe the strength of unsaturated soil in a wide suction range.

Keywords: unsaturated soil; shear strength; soil-water retention curve; effective stress coefficient; wide suction range

1 Introduction

In the regions with expansive soils, landslides frequently occur on highway and canal slopes^[1]. Shear strength is a crucial parameter for assessing slope stability, particularly in relation to the suction of shallow soil, which changes continuously with seasonal wet-dry cycles. This change in suction can influence the shear strength of the soil and the stability of slopes accordingly. To evaluate the impact of climatic conditions on the stability of unsaturated expansive soil slopes, it is essential to quantitatively predict the shear strength of unsaturated soil and its variation with water content^[2].

The key challenge in predicting the shear strength of unsaturated soil lies in how to reasonably consider the influence of suction or saturation on shear strength. Various shear strength models have been proposed to date^[3]. Given the successful application of the effective stress principle in saturated soil, Bishop^[4] extended the effective stress concept to unsaturated soil and proposed the shear strength equation for unsaturated soil as follows:

$$\tau_f = c' + [(\sigma - u_a) + \chi(u_a - u_w)] \tan \varphi' \quad (1)$$

where τ_f represents the shear strength; c' represents the cohesion; χ represents the effective stress coefficient; φ' represents the internal friction angle; u_a represents the pore air pressure; u_w represents the pore water pressure; and σ represents the total stress. In general, assuming that the cohesion and internal friction angle are fixed values,

the accuracy of predicting the shear strength of unsaturated soil can be improved by adjusting the effective stress coefficient. Therefore, varying definitions and determination methods of the unsaturated effective stress coefficient can lead to different prediction results^[5–8]. For the unsaturated soil, when analyzing the stress in multiphase porous media, it is essential to recognize that the air-water interface is an independent phase. This confirms that the influencing mechanisms of net normal stress and matric suction on the mechanical properties of unsaturated soil are different. Using two mutually independent stress variables, Fredlund et al.^[9] derived a shear strength model for unsaturated soil as follows:

$$\tau_f = c' + (\sigma - u_a) \tan \varphi' + (u_a - u_w) \tan \varphi^b \quad (2)$$

where φ^b represents the internal friction angle related to the matric suction. When Eq. (2) is used, φ^b changes with the matric suction, and it is difficult to accurately determine this value. Therefore, Eq. (2) has not been well applied in practice. In fact, the shear strength equations proposed by Bishop^[4] (Eq. (1)) and by Fredlund et al.^[9] (Eq. (2)) are formally consistent and can be transformed

using $\chi = \frac{\tan \varphi^b}{\tan \varphi'}$.

Soil-water interaction is generally classified into capillary and adsorptive effects, which have different effects on the hydraulic properties of water. Bishop’s unsaturated soil strength formula, Fredlund’s unsaturated soil strength formula, and related extended formulae do

Received: 28 December 2022

Accepted: 31 March 2023

This work was supported by the National Natural Science Foundation of China (42307236, 12172187), the Natural Science Foundation of Shandong Province (ZR2023QE001) and the Open Research Fund of State Key Laboratory of Geomechanics and Geotechnical Engineering (SKLGME021019).

First author: Niu Geng, male, born in 1991, PhD, Lecturer, mainly engaged in unsaturated soil mechanics research. E-mail: niugeng@qut.edu.cn.

not differentiate between capillary and adsorptive effects. These models also tend to be more accurate in predicting at low suction ranges but less ideal at high suction ranges. Subsequently, many scholars have attempted to establish unsaturated soil shear strength models that consider both capillary and adsorptive effects^[7–8]. However, their predictive effectiveness in a wide suction range remains less than ideal.

In recent years, experimental research on the strength of unsaturated soil has made significant progress due to the emergence of advanced test instruments. For example, Zhan et al.^[10] utilized a newly developed double-chamber unsaturated soil triaxial apparatus to investigate the influence of suction on the shear strength and shear dilation characteristics of unsaturated expansive soil. Zheng et al.^[11] studied the strength and deformation characteristics of unsaturated soil using a triaxial apparatus that is capable of measuring the local deformation. Zhang et al.^[12] investigated the stress-strain relationship and volumetric changes of expansive soil in a wide suction range using a triaxial

apparatus and the vapor equilibrium method. Due to limitations inherent in the test instruments themselves, most triaxial tests on the unsaturated soil are constrained to suctions below 500 kPa^[12–13], and there are relatively few reports on triaxial tests in the high suction range^[14].

Given the aforementioned issues, this study conducted triaxial tests on unsaturated soil within a wide suction range. We proposed an SWRC model that distinguishes capillary water from adsorbed water. Based on this, a strength formula suitable for a wide suction range of unsaturated soil was proposed. The accuracy of the proposed model was validated using experimental data.

2 Triaxial shear tests

2.1 Test materials and instruments

The weakly expansive soil sampled from the Nanyang section of the South-to-North Water Diversion Central Route Project was used in this study. The basic physical properties are listed in Table 1.

Table 1 Geotechnical properties of Nanyang weakly expansive soil

Specific gravity	Liquid limit /%	Plastic limit /%	Plasticity index	Shrinkage limit /%	Maximum dry density /(g · cm ⁻³)	Optimum water content /%	Free swelling ratio /%
2.74	38.8	17.2	21.6	10.5	1.69	18.2	53.8

For the water retention test, the specimens with initial water content of 22% and dry density of 1.25 g/cm³ were prepared, and then the specimens were saturated with constant volume and fully balanced for future use. For the measurement of soil-water retention curve (SWRC), the pressure plate instrument and saturated salt solution method were used to measure the water retention curves in the low and high suction ranges, respectively.

For the triaxial test on the unsaturated soil, the triaxial specimens with initial water content of 22% and dry density of 1.25 g/cm³ (38 mm in diameter and 76 mm in height) were prepared and compacted in four layers according to the method of controlling height. The unsaturated soil triaxial apparatus produced by GDS Company from the UK was used in the triaxial test, which is equipped with a new type of two-chamber volume change measurement system with bottle-shaped internal chamber. The basic working principle is to obtain the volume change of the specimen by measuring the change of water level (pressure difference) in the internal pressure chamber.

2.1 Test method

2.2.1 Water retention test

The SWRC for a low suction range was measured using the pressure plate instrument, which can control the suction range of 0–1.5 MPa and the suction levels of 10, 20, 40, 80, 150, 300, 600, 900 and 1 300 kPa. After each stage was stabilized under each suction level, the mass and volume of the specimens were measured (the volume was measured by vernier caliper), and then the

next suction level was applied. For the high suction range, the suction was controlled by the vapor equilibrium method, and the specimen prepared with the core cutter method was divided into eight cakes. Two cakes were placed on the ceramic sieve of each moisturizing cylinder. One cake was used to measure the water content, and the other was used to measure the volume. The volume of the cake was measured by Archimedes principle^[15]. Eleven suction levels were selected for high suction range, and the relevant salt solutions and corresponding suctions can be found in the study of Gao et al.^[16]. When the ambient temperature was controlled at 20 °C for 40 d, the mass and volume of the specimen were measured after the specimen reached equilibrium.

2.2.2 Triaxial test

The suction can be classified into low and high categories. For the triaxial tests in the low suction range (0.05, 0.20 and 0.40 MPa), suction equilibrium, consolidation, and triaxial shear were performed in the pressure chamber of the triaxial instrument. This type of test is considered as a drained test with constant suction maintained throughout the testing process. For the triaxial tests in the high suction range, suction equilibrium was conducted outside the triaxial pressure chamber. Consolidation and shear were then performed in the pressure chamber. This type of test is considered as an undrained test with constant water content. For the specimens with suctions of 0.80 and 2.50 MPa, the corresponding gravimetric water contents were obtained according to the SWRC. The mass of the

test specimen was measured in real-time during dehumidification until the target water content was reached. Dehumidification was then stopped, and the specimens were wrapped with plastic film and kept at a constant temperature of 20 °C for 3 d. The volume and water content of the specimens were measured before being placed into the triaxial apparatus for consolidation. A net confining pressure of 100 kPa was applied before shearing. The prepared specimens with suctions of 3.29, 38.00 and 367.00 MPa underwent suction equilibrium in a humidifying cylinder with the relevant salt solution (see Fig. 1). Subsequently, they were consolidated and sheared in a pressure chamber. The salt solution used for the test is listed in Table 2. The axial shear rate for all triaxial shear tests was approximately 0.001 92 mm /min to fully dissipate the pore water pressure during the shear process.



Fig. 1 Equilibrium of suction for sample using vapor equilibrium method

Table 2 Saturated salt solutions and corresponding suctions (20 °C)

Saturated salt solution	Relative humidity /%	Suction /MPa
LiBr	6.6	367.54
NaCl	75.5	38.00
K ₂ SO ₄	97.6	3.29

In the high suction range (suction $s = 0.80, 2.50, 3.29, 38.00$ and 367.00 MPa), the undrained (equal water content) unsaturated soil triaxial test is considered as the equal-suction unsaturated soil triaxial test. This treatment is reasonable because the effect of void ratio on the water retention properties is essentially negligible in the high suction range. For the five tests with high suction, a rubber membrane was sandwiched between the vitrified clay plate in the pressure chamber of the triaxial apparatus and the bottom surface of the specimen to disconnect the drainage channel in order to achieve no drainage during consolidation and triaxial shear processes. The triaxial test paths for all suction ranges are detailed in Fig. 2 (where q is the shear stress and σ_{3n} is the net confining pressure). The initial pressure state was the same for all specimens, and the suction at this point was measured to be approximately 0.17 MPa using WP4, and then suction equilibrium,

consolidation and shear were carried out in this state with different stress paths.

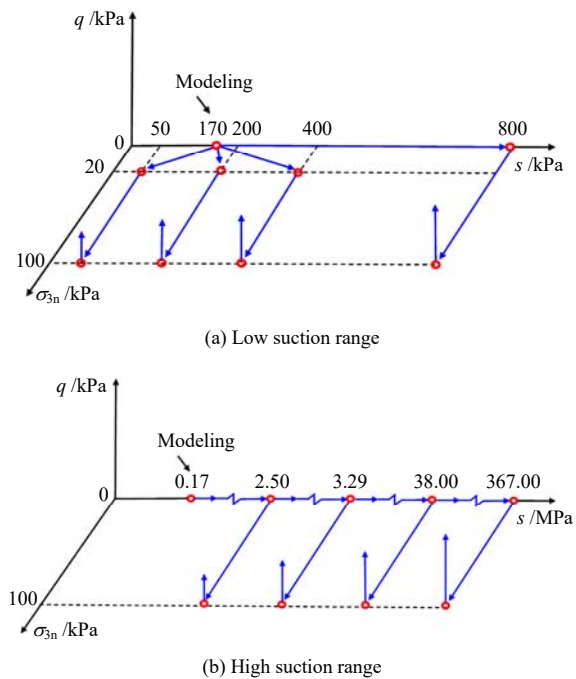


Fig. 2 Stress and suction paths for triaxial tests

3 Test results and analysis

Figure 3 shows the SWRC and void ratio change during the drying process of Nanyang weakly expansive soil with a dry density of 1.25 g/cm^3 . As shown in Fig. 3, the SWRC follows a classical single-peak pattern. The low dry density of the specimen results in a relatively low air entry value (AEV). The trend of void ratio changing with suction follows an inverted S-shape, which is consistent with the typical SWRC. It is important to note that the majority of shrinkage in the mud specimens during the drying process occur before reaching the AEV. However, in the case of compacted specimens, most of the shrinkage occurs between the AEV and the residual value (RV). The difference between the two soil specimens is mainly due to the different pore structures. Additionally, the compacted specimens have a specific structural nature, which causes shrinkage within a relatively larger suction range.

The triaxial test results are shown in Figs. 4 and 5. It can be seen from Fig. 4 that for the specimens with suctions of 0.05, 0.20, 0.40 and 0.80 MPa, the stress q increases with the increase in axial strain ϵ_1 and there is no inflection point and peak value in the whole process. For the specimens with suctions of 2.50 and 3.29 MPa, the stress increases with the increase in axial strain at the initial stage, but when the axial strain reaches about 3%, the stress increase rate slows down and finally tends to be stable. Thus, there will be an inflection point in the stress–strain curve throughout the process. For the specimens with suctions of 38.00 and 367.00 MPa, the stress increases

rapidly with the increase in axial strain at the initial stage, but when the axial strain reaches 2%, the stress decreases rapidly with the increase in axial strain and finally tends to be stable. When it reaches the final stable state, the deviatoric stresses (residual strength) of the specimens with the above two suctions are consistent. In other words, the stress–strain relationship of the specimens with suctions of 0.05, 0.20, 0.40, 0.80, 2.50, and 3.29 MPa is of strain

hardening, and the specimen shows strain hardening and then strain softening until the suction reaches 38.00 and 367.00 MPa. For the peak stress–strain curve, the peak stress is taken as the shear strength of the specimen, and for the non-peak specimen, the stress corresponding to 15% axial strain is taken as the shear strength. Within the whole suction range, the strength of the specimen increases as the suction increases.

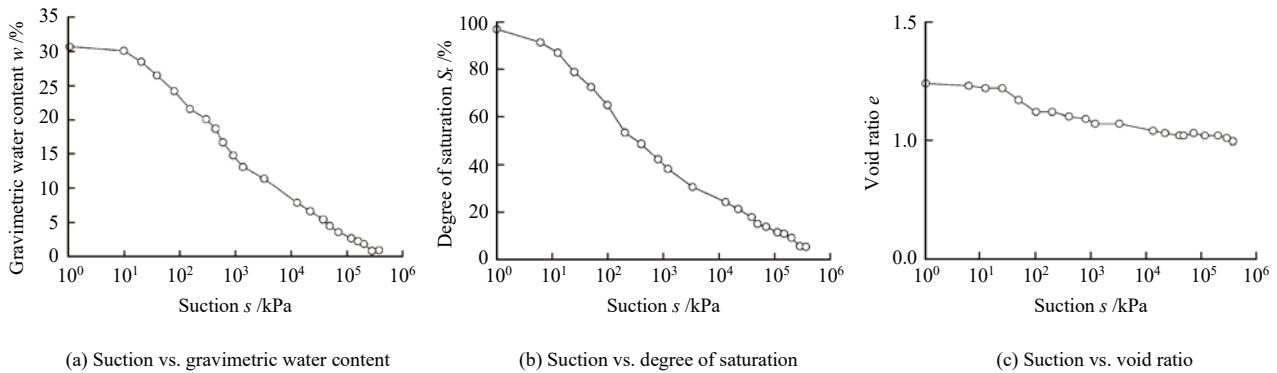


Fig. 3 Soil–water retention curves for Nanyang weakly expansive soil

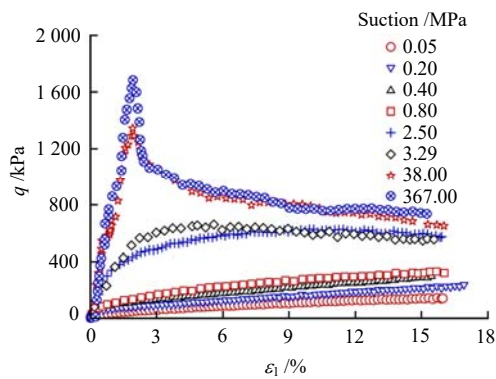


Fig. 4 Relationships between stress and axial strain

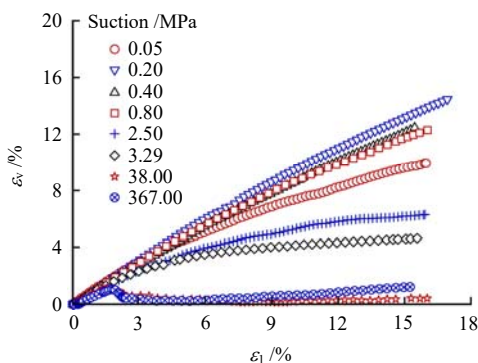


Fig. 5 Volumetric strains in shear test

Figure 5 shows the relationship between volumetric strain ε_v and axial strain ε_1 during the shear test. It can be seen from the figures that the specimens with suction of 0 to 3.29 MPa show a shear contraction during the shear process. However, for the specimens with suctions of 38.00 and 367.00 MPa, although there is still a phenomenon of shear

contraction during the shear process, the axial strain begins to show a trend of shear dilation when the axial strain reaches 2%. It is worth noting that the shear contraction of the specimen with suction of 0.05 MPa is smaller than that of the specimen with suctions of 0.20, 0.40 and 0.80 MPa. The main reason is that the initial dry density of the specimen is relatively small and it is easy to produce compression under the confining pressure. Moreover, compared with other specimens with different suctions, the elastic modulus of the specimen with suction of 0.05 MPa is relatively low, thus the dry density of the specimen after consolidation equilibrium is relatively large, and the shear deformation is relatively small in the shear process. In conclusion, the shear contraction of the specimen becomes lower when the suction increases from 0.20 MPa to 367.00 MPa.

Figure 6 shows the failure pictures of the specimens after shear test. The specimen with suction of 0.80 MPa has no obvious dislocation during the whole triaxial test. This indicates that there is no sliding failure in the shear process, which corresponds to the fact that the stress–strain relationship has always been strain hardening. The specimen



(a) Suction of 0.80 MPa (b) Suction of 2.50 MPa (c) Suction of 367.00 MPa

Fig. 6 Shear failure patterns of soil samples with different suctions

with suction of 2.50 MPa has a certain dislocation on the surface and inside, but there is basically no obvious displacement between the two separate parts. This indicates that the shear plane has not been completely connected, which is consistent with the phenomenon that the stress–strain curve remains unchanged at the later stage of shear test. For the specimen with suction of 367.00 MPa, the shear plane appears at the end of shear test, and the specimen is completely cut into two parts, which corresponds to the strain softening in the stress–strain curve^[15].

According to the above-mentioned phenomenon, it is inferred that in the low suction range, the shear contraction always occurs in the specimen, and there is no obvious relative sliding. In the middle suction range, when the axial strain is small, the shear contraction occurs, and there is no local sliding trend. When the strain reaches a certain value, the local part starts to dislocate, and then the shear dilation occurs. In the high suction range, the shear contraction occurs when the axial strain is small. When the strain reaches a certain value, the inner part of the specimen begins to slip and will continue to develop until the specimen is completely cut into two parts. Therefore, the stress–strain relationship of the specimen is inevitably related to its shear morphology^[15].

4 Shear strength models of unsaturated soil

4.1 Strength formula based on SWRC

According to Eq. (1), the strength formula q_f of unsaturated soil under triaxial stress can be expressed as

$$q_f = \frac{3}{3 - M} \left[c' \frac{6 \cos \varphi'}{3 - \sin \varphi'} + M (\sigma_{3n} + \chi s) \right] \quad (3)$$

where s is the suction calculated by $u_a - u_w$; $M = 6 \sin \varphi' \cdot (3 - \sin \varphi')$, which is the slope of the failure line on the mean stress versus deviatoric stress plane. When Eq. (3) is used, assuming that the internal friction angle and cohesion are fixed, the accuracy of the strength model depends on the effective stress coefficient.

Accurately determining the effective stress coefficient χ is crucial for accurate calculation in the application of effective stress in unsaturated soil. Initially, the global degree of saturation S_r was used to express the effective stress coefficient of unsaturated soil^[17], which can be described by the VG model^[18], and the variation curve of the effective stress coefficient with suction can be obtained as follows:

$$\chi = S_r(s) = \left\{ 1 + \left(\frac{s}{b} \right)^{n_f} \right\}^{-m_f} \quad (4)$$

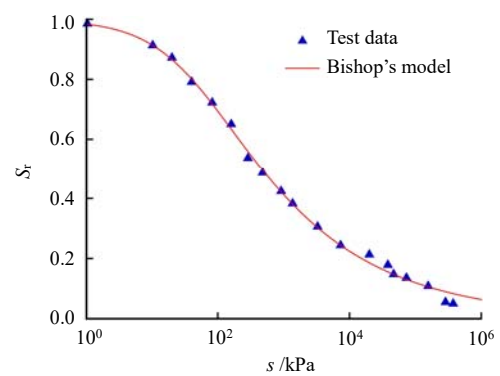
where b , n_f and m_f are the fitting parameters, which can be determined to be 43.6, 0.813 and 0.337 by using Eq. (4) to fit the water retention data of the Nanyang weakly expansive soil, as shown in Fig. 7(a). By substituting Eq. (4) and the fitting parameters into Eq. (3), the relationship between shear strength and suction is obtained, as shown

in Fig. 7(b). It can be found that the calculation results are more accurate in the low suction range, while in the high suction range, this method overestimates the contribution of suction to the effective stress.

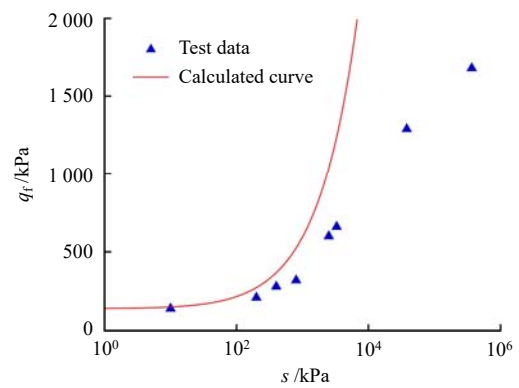
Vanapalli et al.^[5] indicated that the contribution of residual water content to soil strength can be ignored, and the effective stress coefficient χ can be corrected by the effective degree of saturation S_r^e (deducting residual degree of saturation):

$$\chi = S_r^e = S_r(s) - S_r^r \quad (5)$$

where S_r^r is the residual degree of saturation, which can be determined to be about 15% according to Fig. 3.



(a) SWRC



(b) Relation curve between shear strength and suction

Fig. 7 Bishop's shear strength model

The relationship between the effective stress coefficient and suction obtained by using Eq. (5) is shown in Fig. 8(a). By substituting Eq. (5) and the parameters into Eq. (3), the shear strength q_f can be calculated, as shown in Fig. 8(b). One can see that this method is in a good agreement with the experimental data in the low suction range, while in the high suction range, the calculated results are lower than the experimental data.

Khalili and Khabbaz^[6] used the power function of matrix suction to express the effective stress coefficient:

$$\chi = \left(\frac{s}{S_a} \right)^{-0.55} \quad (6)$$

where s_a is the AEV, which is determined to be about 30 kPa according to Fig. 3. The relationship between the effective stress coefficient and suction obtained by using Eq. (6) is shown in Fig. 9(a). The shear strength q_f can be calculated by substituting Eq. (6) and the parameters into Eq. (3), and the result is shown in Fig. 9(b). It can be seen that the calculated results of this method are improved to a certain extent in the high suction range, but the accuracy is still not satisfactory, and the evolution trend of the prediction curve is inconsistent with the experimental data.

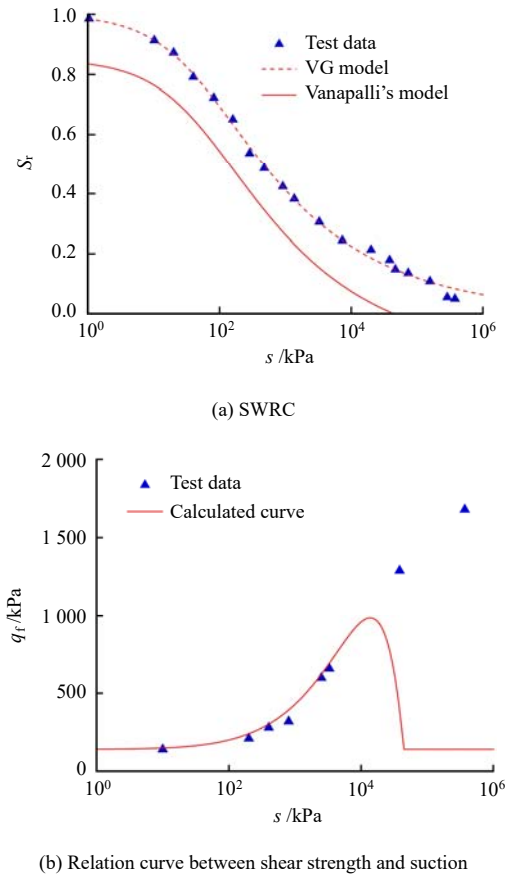


Fig. 8 Vanapalli's shear strength model

If the degree of saturation is used to describe the effective stress coefficient, it is necessary to select a suitable SWRC model to describe the relationship between the effective stress coefficient and suction. Soil-water interaction can be classified into capillary and adsorptive effects. It is found that the capillary and adsorptive effects on the strength of unsaturated soil are different. Therefore, many scholars have proposed to divide the pore water into adsorbed water and capillary water to describe the hydro-mechanical behaviors of unsaturated soil, such as Or et al.^[19], Konrad et al.^[20] and Lu^[21].

The distribution and flow of pore water in the irregular pores are the main factors that affect the hydraulic behaviors of unsaturated soil. With the increase in suction, the water in the irregular pores between soil particles will be discharged, and the pores between particles will become unsaturated.

At this time, the pore water between the soil particles will form a large number of curved liquid surfaces, as shown in Fig. 10(a). With the further increase in suction, the capillary water in the form of curved liquid surface in the irregular pores gradually decreases, while the adsorbed water in the form of adsorbed water film gradually increases. Finally, the pore water primarily exists as adsorbed water, as shown in Fig. 10(b).

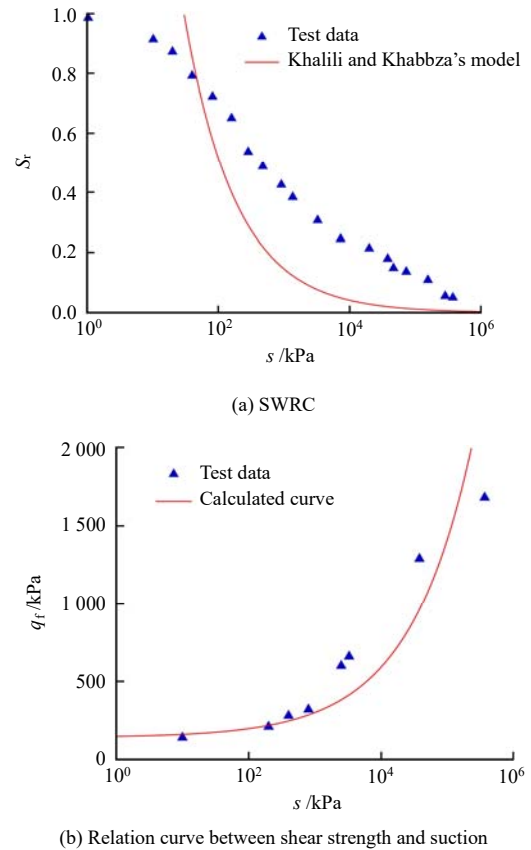


Fig. 9 Khalili and Khabbaz's shear strength model

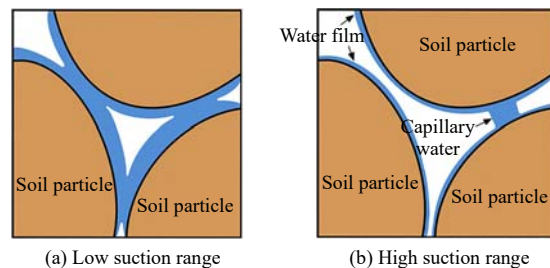


Fig. 10 Schematic diagrams of pore water changes with increasing suction

Therefore, it is reasonable to classify pore water into adsorbed water and capillary water to describe the soil-water retention characteristics of unsaturated soil, and the degree of saturation S_r can be expressed as

$$S_r = S_r^a + S_r^c \quad (7)$$

where S_r^a is the degree of saturation for the adsorbed water; and S_r^c is the degree of saturation for the capillary water. According to the model proposed by Zhou et al.^[7],

we have

$$\chi = S_r^c = \frac{C(s) - \alpha_f C(s) \cdot A(s)}{1 - \alpha_f C(s) \cdot A(s)} \quad (8)$$

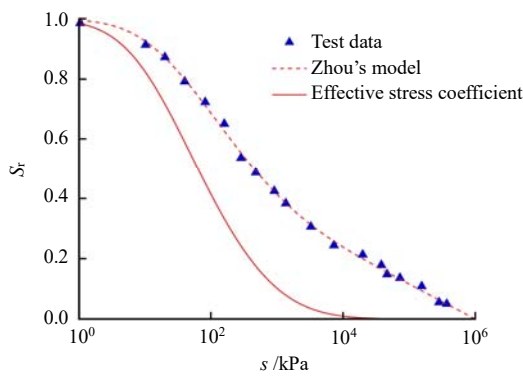
$$S_r^a = \frac{\alpha_f A(s) - \alpha_f C(s) \cdot A(s)}{1 - \alpha_f C(s) \cdot A(s)} \quad (9)$$

$$S_r = S_r^c + S_r^a = \frac{C(s) + \alpha_f A(s) - 2\alpha_f C(s) \cdot A(s)}{1 - \alpha_f C(s) \cdot A(s)} \quad (10)$$

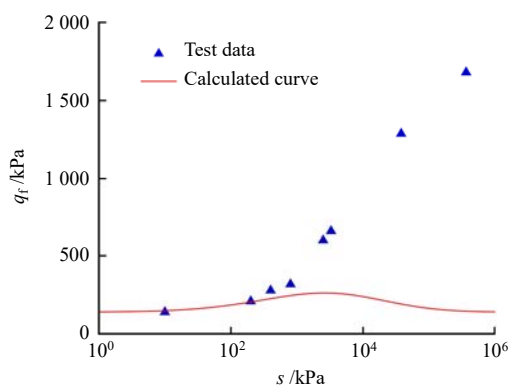
$$C(s) = \frac{1}{2} \operatorname{erfc} \left[\frac{\ln(s/s_m)}{\sqrt{2}\xi} \right] \quad (11)$$

$$A(s) = 1 - \frac{\ln s}{\ln s_d} \quad (12)$$

where s_m is the suction corresponding to the mesopore; s_d is the suction corresponding to the drying state, and $s_d = 10^6$ kPa; ξ is the standard deviation of the pore radius after logarithmic transformation; and α_f is the parameter related to the degree of saturation for the adsorbed water. The above formula is used to fit the soil-water test data as shown in Fig. 11(a), in which the fitting parameters s_m , ξ and α_f are 138.9, 0.529 3 and 0.696, respectively, and the shear strength q_f is obtained by substituting Eq. (8) and the above parameters into Eq. (3). The calculated results are shown in Fig. 11(b). It can be seen that this model performs better in the low suction range, but the calculated curve is obviously lower than the experimental data in the high suction range.



(a) SWRC



(b) Relation curve between shear strength and suction

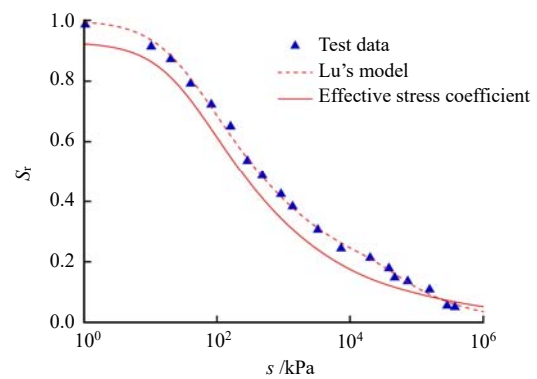
Fig. 11 Zhou's shear strength model

Lu^[21] also proposed an SWRC model to distinguish the capillary water from the adsorbed water:

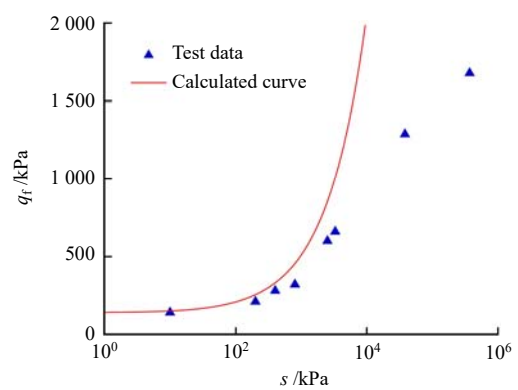
$$S_r^c(s) = [S_s - S_r^a(s)] \left[1 + (\alpha_{nL} s)^{n_{nL}} \right]^{-m_{nL}} \quad (13)$$

$$S_r^a(s) = S_{r_{max}}^a \left\{ 1 - \left[\exp \left(-\frac{s_{max}}{s} \right) \right]^{m_{nL}} \right\} \quad (14)$$

where S_s is the degree of saturation for the saturated soil, which is 100%; $S_{r_{max}}^a$ is the maximum degree of saturation for the adsorbed water; s_{max} is the maximum suction; and α_{nL} , n_{nL} and m_{nL} are the fitting parameters. Using the above equations to fit the soil-water test data, and assuming that the effective stress coefficient is equal to degree of saturation for the capillary soil, the effective stress coefficient is shown in Fig. 12(a). The fitting parameters $S_{r_{max}}^a$, s_{max} , α_{nL} , n_{nL} and m_{nL} are equal to 0.095 92, 5.803 kPa, 71.32, 3.196 and 0.098 38, respectively. Eq. (13) is substituted into Eq. (3) to calculate the shear strength q_f , as shown in Fig. 12(b). It appears that the model is applicable in the low suction range, while in the high suction range, the calculated curve is higher than the experimental data.



(a) SWRC



(b) Relation curve between shear strength and suction

Fig. 12 Lu's shear strength model

Konrad and Lebeau^[20] proposed an SWRC model to distinguish between the capillary water and adsorbed water:

$$S_r = S_r^c + (1 - S_r^c) S_r^a \quad (15)$$

The degrees of saturation for the capillary water S_r^c

and for the adsorbed water S_r^a are written as

$$S_r^c = \begin{cases} 1 & s \leq s_a \\ 1 - (1 - e^{-A's})^{\alpha_{FK}} & s > s_a \end{cases} \quad (16)$$

$$S_r^a = S_r^o \left[1 - \frac{\ln s}{\ln s_{dry}} \right] \quad (17)$$

$$s_a = s_{dry}^{1-1/S_r^o} \quad (18)$$

where s_{dry} is the suction corresponding to the dry state of the soil specimen, which is equal to about 10^6 kPa; A' and α_{FK} represent the parameters related to the shape and size of the pore size distribution; and S_r^o represents the parameter related to the degree of saturation for the adsorbed water in the saturation state. Equation (15) is used to fit the soil-water test data, the fitting parameters A' , α_{FK} and S_r^o are equal to 0.752 7, 0.373 7 and 0.752 7, respectively. Assuming that the effective stress coefficient is equal to the degree of saturation for the capillary water, the effective stress coefficient is shown in Fig. 13(a). Eq. (16) is substituted into Eq. (3) to determine the curve q_p as shown in Fig. 13(b). It is observed that the calculated curve is much lower than the experimental data in the high suction range.

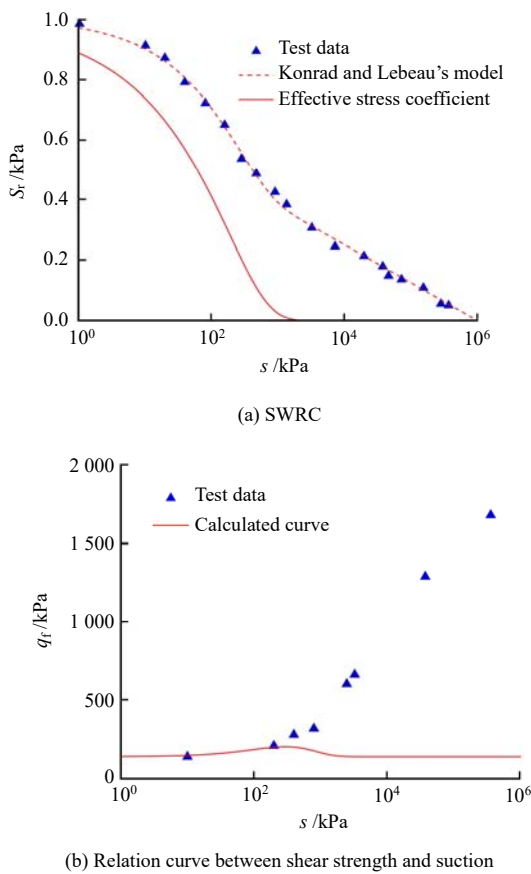


Fig. 13 Konrad and Lebeau's shear strength model

4.2 Improvement of classical strength model

The difference of the shear strength calculated by the

three aforementioned methods using degree of saturation for the capillary water to express the effective stress coefficient is relatively large, and the calculated results are not satisfactory. On the basis of the above calculation, considering the advantages and disadvantages of each model, we try to improve the strength model using following combinations.

4.2.1 Modified model 1

Equations (13) and (17) are substituted into Eq. (7) to describe the SWRC:

$$S_r(s) = [S_s - S_r^a(s)] \left[1 + (\alpha_{FL}s)^{n_{FL}} \right]^{-m_{FL}} + S_r^o \left[1 - \frac{\ln s}{\ln s_{dry}} \right] \quad (19)$$

where

$$S_r^a(s) = S_r^o \left[1 - \frac{\ln s}{\ln s_{dry}} \right] \quad (20)$$

The above equation is used to fit the soil-water test data, and the results are shown in Fig. 14(a). In the fitting process, S_s is 100%, and the fitting parameters S_{rmax}^a , S_{max} , m_{FL} , α_{FL} , n_{FL} and S_r^o are equal to 0.054 22, 1 200 MPa, 0.738, 1, 0.356 1 and 0.663 1, respectively. It is worth noting that the fitting result of this SWRC model is not satisfactory, and there is a certain gap between the calculated results and the experimental data.

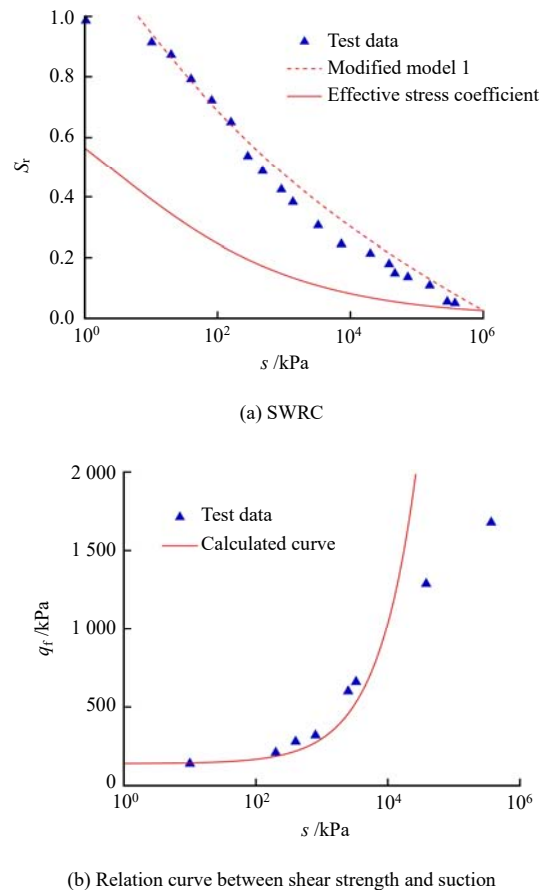


Fig. 14 Modified model 1

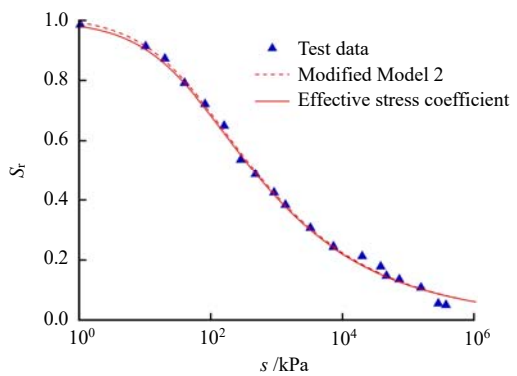
The curve q_f is obtained by substituting $\chi = S_r^c$ into Eq. (3) and the result is shown in Fig. 14(b). It can be seen that in the low suction range, the calculated results are good. However, in the high suction stage, although the calculated results are higher than those before model improvement, the calculated curve is still higher than the experimental data, and the trend predicted by the model is inconsistent with the evolution law of the experimental data.

4.2.2 Modified model 2

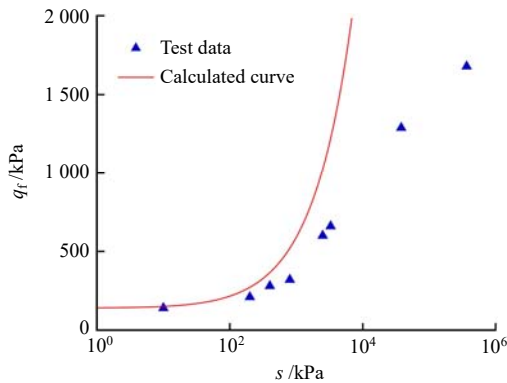
The degree of saturation for the capillary water is expressed by Eq. (4), and the degree of saturation for the adsorbed water is expressed by Eq. (17). Substituting Eqs. (4) and (17) into Eq. (7) results in the SWRC as follows:

$$S_r(s) = \left\{ 1 + \left(\frac{s}{b} \right)^{n_f} \right\}^{-m_f} + S_r^o \left[1 - \frac{\ln s}{\ln s_{dry}} \right] \quad (21)$$

Equation (21) is used to fit the soil-water test data, and the fitting parameters b , n_f , m_f and S_r^o are equal to 44.93, 0.364 2, 0.764 7 and 0.012 95, respectively, as shown in Fig. 15(a). $\chi = S_r^c$ is substituted into Eq. (3) to obtain the shear strength q_f , as shown in Fig. 15(b). It is observed that the calculated result is obviously higher than the experimental data in the medium and high suction range.



(a) SWRC



(b) Relation curve between shear strength and suction

Fig. 15 Modified model 2

4.2.3 Proposed model

Through the analysis and comparison of the above

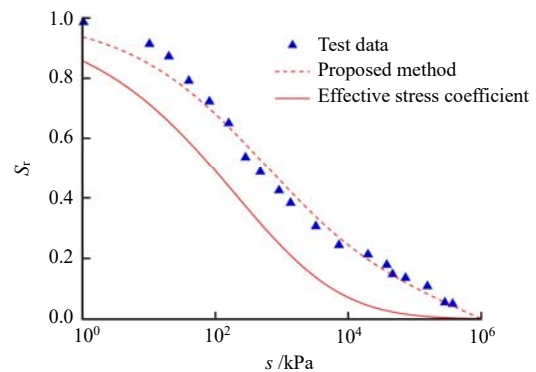
models, it is found that the linear relationship between the degree of saturation for the adsorbed water and the logarithm of suction in the high suction range is more reasonable^[22]. That is to say, Eq. (17) is more accurate to predict the adsorbed water content. Meanwhile, the VG model is improved to address the problem of high degree of saturation for the capillary water in the high suction range:

$$S_r^c(s) = \left[1 + \left(\frac{s}{k} \right)^n \right]^{-\frac{1}{n^m}} \quad (22)$$

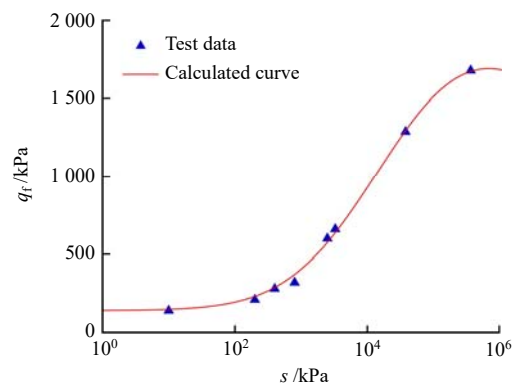
where k is a parameter related to the suction corresponding to the residual water content; n is a parameter describing the rate of soil dewatering; and m is a parameter related to the residual water content. Substituting Eqs. (17) and (22) into Eq. (15), we have

$$S_r(s) = \left[1 + \left(\frac{s}{k} \right)^n \right]^{-\frac{1}{n^m}} + \left\{ 1 - \left[1 + \left(\frac{s}{k} \right)^n \right]^{-\frac{1}{n^m}} \right\} S_r^o \left[1 - \frac{\ln s}{\ln s_{dry}} \right] \quad (23)$$

Equation (23) is used to fit the soil-water test data, and the fitting parameters k , n and m are equal to 6 314, 0.351 3 and 1.415, respectively, as shown in Fig. 16(a). $\chi = S_r^c$ is substituted into Eq. (3) to obtain the shear strength curve q_f , and the calculated result is shown in Fig. 16(b). The results show that the calculated curve is



(a) SWRC



(b) Relation curve between shear strength and suction

Fig. 16 Proposed shear strength model

in a good agreement with the experimental data in a wide suction range, and the variation trend of shear strength with suction is consistent with the experimental data.

Figure 17 shows the shear strength curves predicted by the proposed shear strength model and the classical strength models in the literature and the experimental data. It is observed that in the low suction range, the shear strength obtained by all methods is in a good agreement with the experimental data. However, the shear strengths obtained by the Bishop's method, Khalili and Khabbza's method and Lu's method overestimate the contribution of suction to the shear strength in the high suction range, while the curves calculated by the Vanapalli's method, Zhou's method and Konrad and Lebeau's method are lower than the experimental data in the high suction range. Moreover, these methods are inconsistent with the evolution of the experimental data in the high suction range. In a wide suction range, the shear strength curve calculated by the proposed method has a satisfactory agreement with the experimental data, and its evolution law with suction is also consistent.

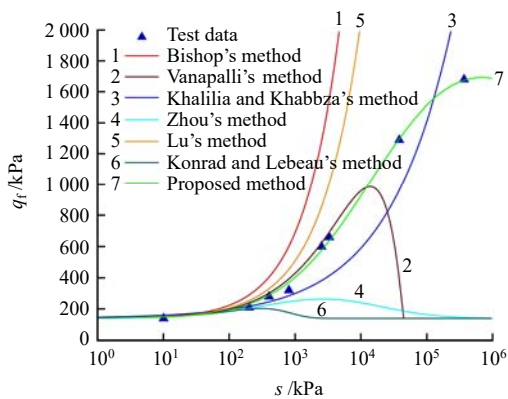
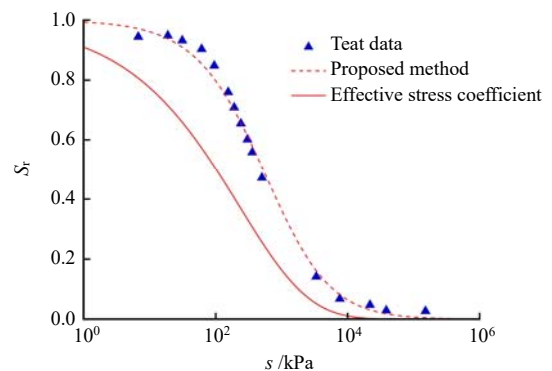


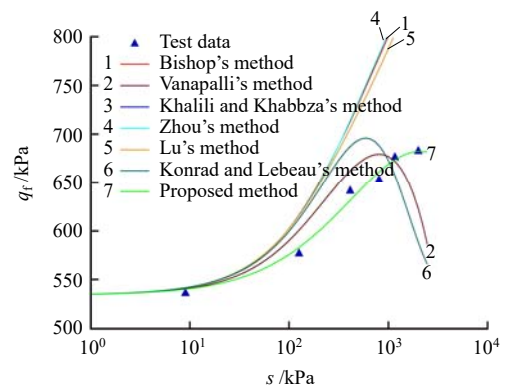
Fig. 17 Comparisons between test data and predicted results from different prediction models

In order to further verify the validity of the proposed model, the shear strength data of Madrid sand with clay particles^[23] and Botkin silty clay^[24] are used for calculation and comparison. Figure 18 shows the calculated results

of Madrid sand with clay particles, and it can be seen that the fitted SWRC is in a good agreement with the experimental data. Meanwhile, the proposed shear strength model can well describe the shear strength behavior of Madrid clay sand in a wide suction range. Figure 19(a) shows the measured SWRC of Botkin silty clay and the fitting curve, and it is also observed that the fitting results are very good. Figure 19(b) shows the measured shear strength and calculated results, and it is observed that the calculated results by the model well coincide with the experimental data of all models.

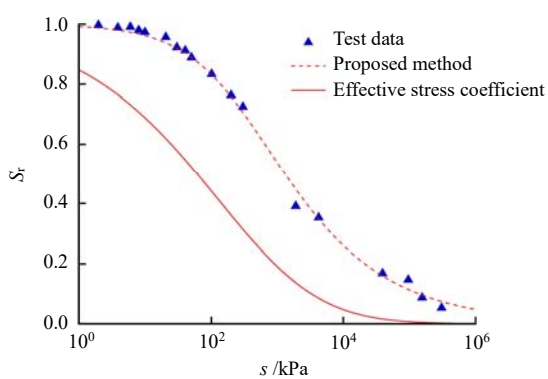


(a) SWRC

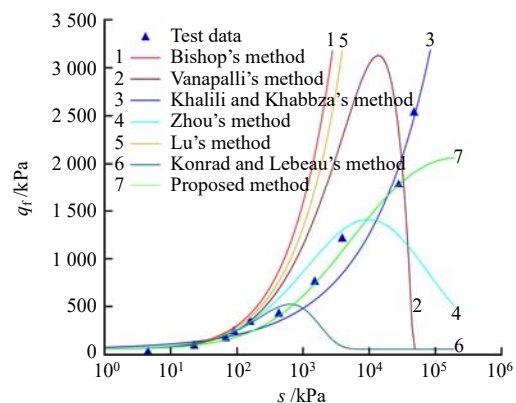


(b) Shear strength

Fig. 18 Test data and predicted results for Madrid clayey sand (data from Escario^[23])



(a) SWRC



(b) Shear strength

Fig. 19 Test data and predicted results for Botkin silt clay (data from Vanapalli et al.^[24])

5 Conclusions

(1) The triaxial shear tests were carried out on the Nanyang weakly expansive clay in a wide suction range. In the low suction range, the specimen shows shear contraction, while in the high suction range, the specimen begins to show shear dilation at 2% axial strain.

(2) In the wide suction range, the stress–strain curve increases with the increase in suction. Strain hardening occurs in the low suction range, while strain softening appears in the high suction range. There is a close relationship between the stress–strain type and the shear failure pattern of the specimen.

(3) An SWRC model to distinguish the capillary water from the adsorbed water is proposed, and the effective stress coefficient is expressed by the degree of saturation for the capillary water. On this basis, a shear strength formula suitable for a wide suction range is proposed. The accuracy of the proposed method is proved by comparing it with the experimental data of different soils and the strength models in the literature.

References

- [1] CHEN Zheng-han, GUO Nan. New developments of mechanics and application for unsaturated soils and special soils[J]. *Rock and Soil Mechanics*, 2019, 40(1): 1–54.
- [2] TANG Chao-sheng. Extrem climate engineering geology: soil engineering properties response to drought climate and measures for disaster mitigation[J]. *China Science Bulletin*, 2020, 65(27): 3009–3027.
- [3] GAO Y, SUN D A, ZHOU A N, et al. Predicting shear strength of unsaturated soils over wide suction range[J]. *International Journal of Geomechanics*, ASCE, 2020, 20(2): 04019175.
- [4] BISHOP A W. The principle of effective stress[J]. *Teknisk Ukeblad*, 1959, 39: 859–863.
- [5] VANAPALLI S K, FREDLUND D G, PUF AHL D E, et al. Model for the prediction of shear strength with respect to soil suction[J]. *Canadian Geotechnical Journal*, 1996, 33(3): 379–392.
- [6] KHALILI N, KHABBAZ M H. A unique relationship for the determination of the shear strength of unsaturated soils[J]. *Géotechnique*, 1998, 48(5): 681–687.
- [7] ZHOU A, HUANG R, SHENG D. Capillary water retention curve and shear strength of unsaturated soils[J]. *Canadian Geotechnical Journal*, 2016, 53(6): 974–987.
- [8] XU Xiao, ZHAO Cheng-gang, CAI Guo-qing. Shear strength of unsaturated soils considering capillary and adsorptive mechanisms[J]. *Rock and Soil Mechanics*, 2018, 39(6): 2059–2064.
- [9] FREDLUND D G, MORGENSTERN N R, WIDGER R A. The shear strength of unsaturated soils[J]. *Canadian Geotechnical Journal*, 1978, 15(3): 313–321.
- [10] ZHAN Liang-tong, NG C W W. Experimental study on mechanical behavior of recompacted unsaturated expansive clay[J]. *Chinese Journal of Geotechnical Engineering*, 2006, 28(2): 196–201.
- [11] ZHENG G, SHAO L, GUO X, et al. Investigation of the mechanical behaviour of an unsaturated soil mixture using a digital image measurement system[J]. *European Journal of Environmental and Civil Engineering*, 2020, 24(8): 1051–1067.
- [12] ZHANG J R, NIU G, LI X, et al. Hydro-mechanical behavior of expansive soils with different dry densities over a wide suction range[J]. *Acta Geotechnica*, 2020, 15(1): 265–278.
- [13] GAO Y, SUN D, ZHU Z, et al. Hydromechanical behavior of unsaturated soil with different initial densities over a wide suction range[J]. *Acta Geotechnica*, 2019, 14(2): 417–428.
- [14] BLATZ J A, GRAHAM J, CHANDLER N A. Influence of suction on the strength and stiffness of compacted sand–bentonite[J]. *Canadian Geotechnical Journal*, 2002, 39(5): 1005–1015.
- [15] LIU Qian-qian, LI Jian, CAI Guo-qing, et al. Experimental study on water retention characteristics of saline soil in the full suction range[J]. *Rock and Soil Mechanics*, 2021, 42(3): 713–722.
- [16] GAO You, LI Ze, SUN De-an, et al. Unimodal and bimodal soil-water characteristic curves model considering the effect of initial void ratio[J]. *Rock and Soil Mechanics*, 2022, 43(6): 1441–1452.
- [17] BISHOP A W, BLIGHT G E. Some aspects of effective stress in saturated and partly saturated soils[J]. *Geotechnique*, 1963, 13(3): 177–197.
- [18] VAN GENUCHTEN M T. A closed-form equation for predicting the hydraulic conductivity of unsaturated soils[J]. *Soil Science Society of America Journal*, 1980, 44(5): 892–898.
- [19] OR D, TULLER M. Liquid retention and interfacial area in variably saturated porous media: upscaling from single-pore to sample-scale model[J]. *Water Resources Research*, 1999, 35(12): 3591–3605.
- [20] KONRAD J M, LEBEAU M. Capillary-based effective stress formulation for predicting shear strength of unsaturated soils[J]. *Canadian Geotechnical Journal*, 2015, 52(12): 2067–2076.
- [21] LU N. Generalized soil water retention equation for adsorption and capillarity[J]. *Journal of Geotechnical and Geoenvironmental Engineering*, 2016, 142(10): 04016051.
- [22] CAMPBELL G S, SHIOZAWAS. Prediction of hydraulic properties of soils using particle-size distribution and bulk density data, in *Indirect methods for estimating the hydraulic properties of unsaturated soils*[M]. Riverside, CA: University of California Riverside, 1992: 317–328.
- [23] ESCARIO V. Strength and deformation of partly saturated soils[C]//*Proceedings of the 12th International Conference on SMFE*. [S. l.]: [s. n.], 1989, 1: 43–46.
- [24] VANAPALLI S K, WRIGHT A, FREDLUND D G. Shear strength behavior of a silty soil over the suction range from 0 to 1 000 000 kPa[C]//*Proceedings of the 53th Canadian Geotechnical Conference*. Montreal, CA: [s. n.], 2000: 15–18.